Geoderma Regional 2–3 (2014) 82–90

Contents lists available at ScienceDirect

Geoderma Regional

journal homepage: www.elsevier.com/locate/geodrs

Regional scale soil salinity evaluation using Landsat 7, western San Joaquin Valley, California, USA

Elia Scudiero *, Todd H. Skaggs, Dennis L. Corwin

USDA-ARS, United States Salinity Laboratory, 450 West Big Springs Rd., Riverside, CA 92507-4617, USA

ARTICLE INFO

Article history:
Received 21 July 2014
Received in revised form 17 October 2014
Accepted 21 October 2014
Available online 24 October 2014

Keywords:
Aridisols
Entisols
Inceptisols
Mollisols
Vertisols
Spatial variability
Apparent soil electrical conductivity
Remote sensing

ABSTRACT

Despite decades of research in soil mapping, characterizing the spatial variability of soil salinity across large regions remains a crucial challenge. This work explores the potential use of Landsat 7 (L7) satellite reflectance data (30 × 30 m resolution) to facilitate salinity mapping. Reflectance data spanning a seven-year period (2007–2013) were obtained for western San Joaquin Valley, California (ca. 1.5×10^6 ha), over five soil Orders (Aridisols, Entisols, Inceptisols, Mollisols, and Vertisols). Two ground-truth datasets were considered: 267 direct measurements of salinity (one per L7 pixel) from soil samples (EC_e), and 4891 indirect salinity values (EC_e^*) estimated from the relationships of EC_e with geospatial (on average 16 per L7 pixel) electromagnetic induction measurements. The EC_e^* ground-truth dataset was characterized by stronger relationship with the L7 reflectance, with the multi-year averages of the L7 data showing R^2 up to 0.43. The correlations between L7 data and EC_e^* were significantly influenced by rainfall (stronger in dry years than in rainy years), soil properties (weaker in finer soils), and crop type (stronger when soil salinity was over crop stress tolerance threshold). The results suggest that a fusion of the L7 multi-year reflectance data with information on meteorological conditions, crop type, and soil texture could lead to a reliable salinity prediction model for the entire western San Joaquin Valley. Land resource managers, producers, agriculture consultants, extension specialists, and Natural Resource Conservation Service field staff are the beneficiaries of regional-scale maps of soil salinity.

Published by Elsevier B.V.

1. Introduction

Soil salinization diminishes the productivity of irrigated farmlands throughout the world (Ghassemi et al., 1995; Ivits et al., 2013). Of the cultivated lands worldwide, about 0.34×10^9 ha (23%) are estimated to be saline and another 0.56×10^9 ha (37%) are estimated to be sodic (Tanji and Wallender, 2012). In actuality, these estimates are educated guesses at best as no reliable inventories of soil salinity exist due to the dynamic and complex spatial and temporal nature of salinity, which make measurements at regional scale problematic. The available regional maps are often qualitative or unreliable (Lal et al., 2004; Lobell, 2010), and, therefore, provide little useful information for producers, land and water resource managers, extension specialists, or policy and decision makers. Methods of quantitatively mapping and monitoring soil salinity at regional to global scales are essential to provide land and water resource managers with the information needed to make recommendations to decision makers faced with policy decisions responding to climate pattern changes and increased food demands that require alternative water (e.g., reuse of degraded water) and land (e.g., reclamation of non-productive saline-sodic soils) sources.

Agriculturally rich areas, such as California's San Joaquin Valley, are economically impacted with lost revenues of tens to hundreds of millions of dollars each year due to reduced crop yield from salinity (Johnston et al., 2012). The west side of the San Joaquin Valley (WSJV) is particularly susceptible to the accumulation of salinity due to shallow water tables and native levels of salts (Letey, 2000). Maps inventorying salinity and monitoring the spatio-temporal changes in salinity for the WSJV are vital to the management of salinity and allocation of limited water resources, particularly during recurring periods of drought. Recent advances in the use of satellite imagery (Metternicht and Zinck, 2003; Caccetta et al., 2010; Furby et al., 2010; Lobell et al., 2010; Singh et al., 2010) and electromagnetic induction (Corwin and Lesch, 2014) have made positive strides in regional-scale salinity assessment.

Ground-based geospatial measurements of apparent electrical conductivity (EC_a), from electromagnetic induction, can be obtained relatively quickly and can be used as a proxy for soil salinity (Corwin and Lesch, 2013). Typically, for a field-scale (i.e., tens of hectares) salinity assessment a small number of soil salinity measurements determined from electrical conductivity of the saturation extract (EC_e) are made in conjunction with a larger EC_a survey so that a relationship between EC_a and EC_e can be determined (Lesch et al., 1992; Triantafilis et al.,

* Corresponding author.
E-mail addresses: scudiero@dmsa.unipd.it, elia.scudiero@ars.usda.gov (E. Scudiero).

http://dx.doi.org/10.1016/j.geodrs.2014.10.004
2352-0094/Published by Elsevier B.V.

2000). Corwin and Lesch (2014) proposed a spatial linear regression technique to describe the relationships between salinity and EC_a, based on the analysis of covariance, over very large areas (i.e., tens of thousands of hectares). Once such a relationship is established, a unique regression slope can be used throughout a region, whereas the intercept values would vary at a smaller scale (e.g., field scale), reducing (up to the 60%) the number of soil samples needed to map an entire region.

The size of an area that can be surveyed using ground-based instrumentation is, however, limited due to practical considerations, which leads to consideration of remote sensing. There is great potential in the use of remote sensing for assessing and mapping soil salinity (Lobell, 2010; Allbed and Kumar, 2013). In agricultural areas, the most accurate quantitative remote sensing salinity estimations across a regional scale have been achieved by studying crop canopy reflectance (Lobell et al., 2010). Good results have also been obtained studying bare-soil reflectance, but mainly on lands with very high salinities that cannot be tolerated by most crops (Metternicht and Zinck, 2003; Allbed and Kumar, 2013). Canopy reflectance has been used to represent crop status throughout the growing season and to predict yield (Mulla, 2013). The intra-annual variations in crop reflectance depend on factors influencing plant growth through each year, and are, therefore, a means of monitoring vegetation health rather than discriminating between different stress types (Scudiero et al., 2014). Nevertheless, previous studies showed that landscape features that are relatively stable in time (such as soil salinity) can be emphasized using multi-year reflectance data (Lobell et al., 2010). In fact, using multiple-year satellite data generally improves the reflectance–salinity relationships compared to those observed for a single-year (Lobell et al., 2007, 2010; Furby et al., 2010; Dang et al., 2011; Scudiero et al., 2014). Scudiero et al. (2014) showed that that areas affected by soil salinity are generally characterized by lower temporal variability of canopy reflectance than areas with healthy vegetation, or areas suffering from other stresses that are less stable in time (e.g., water stress, pests…). The research of Lobell et al. (2010) indicated that the multi-year analysis of MODIS (National Aeronautics and Space Administration Agency, USA) reflectance integrated by information on crop cover, could explain large portions (up to 53%) of the spatial variability of soil salinity in the Red River Valley, North Dakota and Minnesota, USA. Unfortunately, MODIS data has very coarse spatial resolution (250 × 250 m), which does not generally allow proper land management at the sub-field scale.

In the United States, regional studies at spatial resolutions high enough to be used by producers (i.e., field or sub-field scale) have not been carried out using remote sensing data. Canopy reflectance obtained from the Landsat 7 (L7) satellite sensor (National Aeronautics and Space Administration Agency and US Geological Survey, USA) could be potentially used for this purpose as characterized by moderately high spatial resolution (900 m^2). In other countries L7 surface reflectance has been used for salinity assessment by various authors (e.g., Furby et al., 2010; Taghizadeh-Mehrjardi et al., 2014) in the past years, often on soils characterized by very high salinity values. In the USA, to our knowledge, the multispectral data from the L7 satellite has not been tested for use in soil salinity assessment on agricultural land, especially at low and moderate salinity levels, where most crops can still grow.

The objective of this study was to explore the use of multi-year Landsat 7 canopy reflectance data for regional-scale salinity assessment in the WSJV. To do so, reflectance–salinity relationships were analyzed over a 7-year period at regional and field scales, using the six Landsat 7 spectral bands and selected vegetation indices. Additionally, the study aimed to understand the spatio-temporal variability of the relationship between canopy reflectance and soil salinity, and to identify possible explanatory variables for a salinity assessment model utilizing L7 reflectance and other ancillary data, such as information on meteorological conditions and soil type.

2. Materials and methods

2.1. Western San Joaquin Valley

The Central Valley of California, which includes the San Joaquin Valley, the Sacramento Valley, and the Sacramento-San Joaquin Delta, produces about 25% of USA's table food on only 1% of the nation's farmland (Cone, 1997). The San Joaquin Valley lies south of the Sacramento–San Joaquin River Delta in California's Central Valley stretching 354 km in length and 64–97 km in width (Fig. 1a). Irrigated land comprises 2.3 × 10^6 ha of the San Joaquin Valley. Saline and saline–sodic soils are estimated to cover 8.9 × 10^5 ha in the San Joaquin Valley, of which most are found in the WSJV (Backlund and Hoppes, 1984). The major crops grown include grapes, cotton, nuts, citrus, garlic, tomatoes, and alfalfa. Cattle and sheep ranching and dairy farming are also important to the valley's agricultural productivity. The soils of the WSJV are derived from alluvium originating from the coastal mountains. The alluvium contains high concentrations of salts since the coastal mountains were once below sea level and uplifted to their present state (Letey, 2000).

The selection of the WSJV as the study site was based on two factors: (i) the tremendous agricultural productivity of this region and the impact that salinity has on that productivity and (ii) the need for a current reliable inventory of salinity to enable water resource managers to make informed water and salinity management decisions, particularly during droughts.

Twenty-two fields across the WSJV were selected (Fig. 1) to provide ground-truth soil salinity data.

2.2. Landsat 7 Surface Reflectance Climate Data Record

The Landsat 7 (L7) satellite sensor (National Aeronautics and Space Administration Agency and US Geological Survey, USA) provides reflectance imagery with a 30 × 30 m resolution over six spectral bands, namely: blue (B, 450–520 nm), green (G, 520–600 nm), red (R, 630–690 nm), near-infrared (NIR, 770–900 nm), shortwave infrared 1 (IR1, 1550–1750 nm), and shortwave infrared 2 (IR2, 2090–2350 nm). The Landsat 7 Climate Data Record (CDR) surface reflectance was used in this study. The L7 CDR is atmospherically corrected through the Landsat Ecosystem Disturbance Adaptive Processing System (LEDAPS) according to Masek et al. (2006). The WSJV is covered by five L7 acquisition areas (Fig. 1). Scenes were obtained from January 2007 through December 2013. A total number of 366 scenes with cloud coverage <10% were considered. The seven years of L7 data consisted of about 13–27 cloudless scenes per year over each ground-truth study site (Table 1). Most of the data was available for the spring, summer, and early fall months, whereas less than 23% of the scenes were from the months of January, February, March, November, and December.

Several vegetation indices were calculated using the L7 spectral bands as suggested by Mulla (2013), Li et al. (2013), and Jiang et al. (2008). Five indices were selected because of their past performances and popularity in the literature. The selected indices were (Table 2): Normalized Difference Vegetation Index, NDVI (Rouse et al., 1973); Enhanced Vegetation Index, EVI (Huete et al., 2002), where the aerosol and soil correcting parameters g, c_1, c_2, and l are set to 2.5, 6, −7.5, and 1, respectively; Salinity Index, SI (Aldakheel et al., 2005); Green Atmospherically Resistant Vegetation Index, GARI (Gitelson et al., 1996), where $\gamma = 0.9$ is a parameter that improves atmospheric correction; and a new index developed in this study, the Canopy Response Salinity Index, CRSI.

The NDVI is well-known and widely used in remote sensing studies (Jackson et al., 2004; Jiang et al., 2008). Lobell et al. (2010) similarly found that the EVI could describe up to half of the spatial variability in soil salinity in a regional-scale salinity assessment using MODIS data. The SI has also been found useful for predicting soil salinity and sodicity (Aldakheel et al., 2005; Odeh and Onus, 2008). The GARI was formulated to enhance the sensing of green vegetation (Gitelson et al., 1996) and

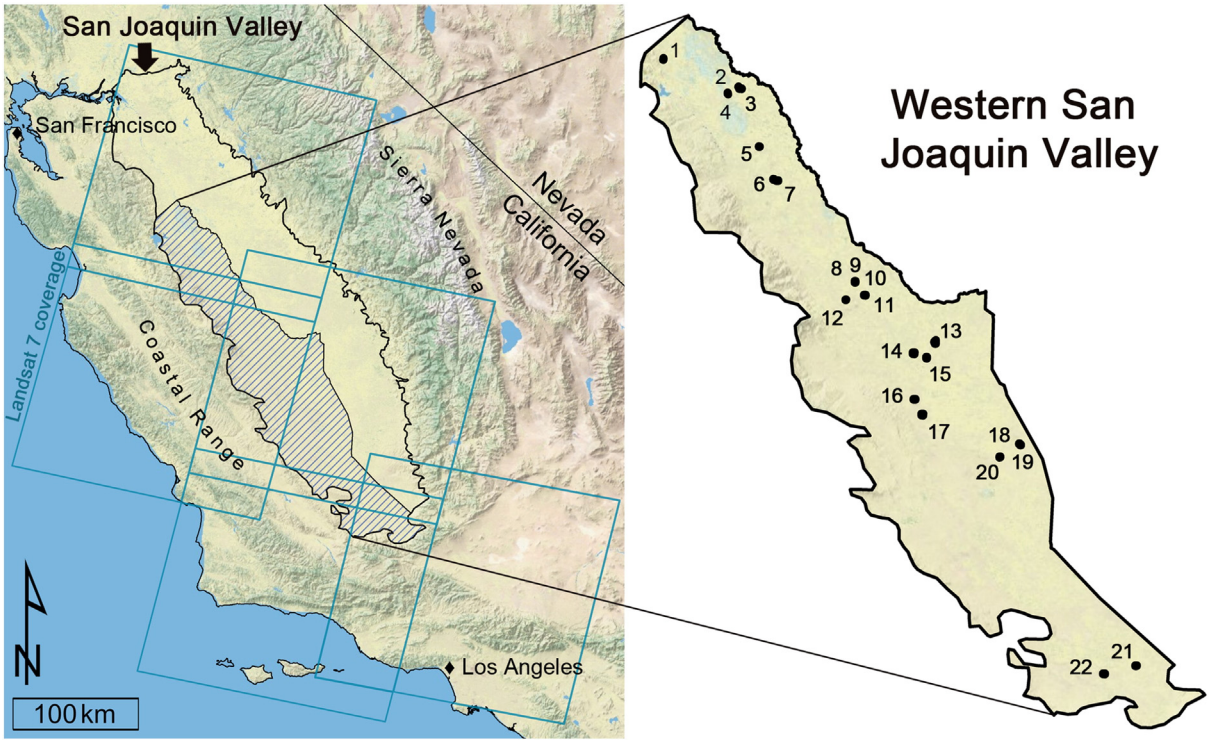

Fig. 1. Map of California's San Joaquin Valley. The western San Joaquin Valley (WSJV) is highlighted with hatch marks. The squares represent the Landsat 7 coverage over the WSJV. The location of the 22 study sites is shown in the detailed WSJV map (right).

proved to be useful for crop coverage assessment studies (Vina et al., 2004). Finally the CRSI was formulated to monitor plant fitness using all the visible and near-infrared bands. Like many vegetation indices (Jiang et al., 2008), the CRSI was formulated to highlight the small peak of reflectance typically observed in the 400–500 nm wavelengths and the sudden change in reflectance occurring between red and near-infrared wavelengths. The formulation of the index was empirical, and CRSI is not associated with any plant physiological property, but with general plant health.

The L7 Scan Line Corrector (SLC) failed in May 31, 2003. The stripes of the L7 SLC-off were masked and the L7 data over each study field were stacked (average) for each entire year similarly to Roy et al. (2010). The yearly L7 mosaics were then averaged over the 7-year time span according to Lobell et al. (2010). Temporal variability maps of the L7 data were also computed according to Eq. (1), as originally proposed by Tweed et al. (2007) when measuring the temporal variations of NDVI:

$$\sigma(U)_j = \sqrt{\frac{1}{N-1} \cdot \sum_{i=1}^{N} (U_i - U_{mean})^2} \quad (1)$$

where σ is the temporal variation of the variable U, calculated at each cell j, over N (=7) years; and U_{mean} and U_i are the 7-year average and 1-year average (mosaic) on year i, respectively.

2.3. Ground-truth datasets

Fig. 1b shows the location of the twenty-two fields that were selected to provide ground-truth soil salinity data. The fields were of various sizes (total area 542 ha, average 24.1 ha, minimum 2.3 ha, and maximum 63.0 ha).

In 2013, the fields were surveyed with intensive electromagnetic induction (EMI) geospatial readings using an EM38 Dual Dipole (Geonics Ltd., Mississauga, Ontario, Canada) sensor connected to a GPS and mounted on a nonmetallic sled following the protocols given by Corwin and Lesch (2013). The EM38 measured soil apparent electrical conductivity (EC_a) at 41,779 locations over the 22 fields (150 to 13,400 readings per field, at an average density of ca 175 measurements per ha^{-1}), for both the 0–0.75 (EC_aH) and 0–1.50 (EC_aV) m soil profiles.

The EC_a readings were analyzed using the ESAP software package (Lesch et al., 2000; Lesch, 2005): the soil sampling scheme delineation was carried out according to the local variations in EC_a across a field

Table 1
Average number of cloudless (<10% cloud coverage) Landsat 7 Climate Data Record scenes available per field in the 2007–2013 time frame.

Year	Average number of cloudless Landsat 7 Climate Data Record scenes available per field												
	Yearly	Jan.	Feb.	Mar.	Apr.	May	Jun.	Jul.	Aug.	Sept.	Oct.	Nov.	Dec.
2007	15.9	0.8	0.6	0.3	2.3	1.5	1.9	1.4	1.4	3.3	1.4	0.1	1.0
2008	17.8	0.0	1.0	1.0	2.0	1.5	2.5	2.0	2.5	1.9	2.6	0.8	0.0
2009	15.5	1.0	1.6	1.0	1.2	1.8	0.9	1.7	1.1	1.3	2.3	1.6	0.1
2010	13.9	0.0	0.1	0.0	1.7	1.4	1.9	2.5	1.9	2.1	0.7	1.5	0.1
2011	14.4	0.0	0.1	0.7	0.8	0.6	1.5	3.1	2.6	2.5	1.0	0.1	1.5
2012	13.3	1.5	1.5	0.0	1.1	0.7	1.9	1.5	1.2	1.5	1.5	0.6	0.2
2013	26.6	0.9	1.8	0.4	2.4	2.4	3.0	2.4	1.6	3.3	2.7	3.1	2.6

Table 2
Vegetation Indices evaluated in the study.

Index	Formulation[a]
Normalized Difference Vegetation Index	$NDVI = \frac{(NIR-R)}{(NIR+R)}$
Enhanced Vegetation Index	$EVI = g \times \frac{(NIR-R)}{(NIR+c_1 \times R - c_2 \times B + l)}$
Salinity Index	$SI = \sqrt{G \times R}$
Green Atmospherically Resistant Vegetation Index	$GARI = \frac{NIR-[G+\gamma \times (B-R)]}{NIR+[G+\gamma \times (B-R)]}$
Canopy Response Salinity Index	$CRSI = \sqrt{\frac{(NIR \times R)-(G \times B)}{(NIR \times R)+(G \times B)}}$

[a] Landsat 7 spectral bands: blue (B), green (G), red (R), near-infrared (NIR), infrared 1(IR1), and infrared 2 (IR2). Aerosol and soil correcting parameters: g, c_1, c_2, l, and γ.

using the Response Surface Sampling Design algorithm (Lesch, 2005). Soil was sampled at 267 locations over the 22 fields (6 to 50 sites per field, average density of 0.42 sample ha^{-1}) at 0–0.3, 0.3–0.6, 0.6–0.9, 0.9–1.2, and 1.2–1.5 m. The soil saturation extract was analyzed for electrical conductivity (EC_e, dS m^{-1}) and pH. The EC_e measurements were used as a first ground-truth dataset for soil salinity. Soil was also analyzed for gravimetric water content (WC) and saturation percentage (SP). Both WC and SP can be used to describe the spatial patterns of textural properties and bulk density (Corwin et al., 2003; Janik, 2008). In particular, even though WC at single locations changes over time, its spatial pattern (i.e., hydrologic signature) remains fairly constant throughout the growing season (Engman, 1999), representing soil water retention capacity.

As a second ground-truth dataset, salinity values were estimated (EC_e^*) at the EMI sampling locations using spatial linear regression models (Lesch and Corwin, 2008), similarly to what was done by Lobell et al. (2010). The EC_e^* estimations were developed on a field-by-field basis, over the 0–1.2 m soil profile (i.e., soil profile with the strongest EC_a–EC_e relationships). For each field the predictor was the EM38 output (i.e., EC_aH or EC_aV) that best correlated with the EC_e data.

Note that the L7 measurements reflect the average characteristics of a 30 × 30 m pixel, therefore, comparisons of field point data with the L7 reflectance require some assumption about how the two spatial scales relate (Lobell et al., 2010). The measured EC_e values were considered to represent an entire 900 m^2 pixel, thus assuming little spatial variability of soil salinity within each L7 pixel. Contrarily, kriging with 30 × 30 m block support was used to interpolate the intensive EMI survey data onto a regular 30 × 30 m grid (Lobell et al., 2010), thereby better accounting for sub-pixel spatial variability of soil salinity. An ordinary kriging with block support was used with an isotropic exponential semivariogram to fit the EC_e^* data over the 30 × 30 m grid using ArcMap 10.1 (ESRI, Redlands, CA, USA).

The differences in reflectance values for the L7 bands over five different salinity intervals were tested. The intervals were 0–2 (non-saline), 2–4 (slightly saline), 4–8 (moderately saline), 8–16 (strongly saline), and above 16 (extremely saline) dS m^{-1}. The differences were tested using the non-parametric Kruskal–Wallis rank test (Kruskal and Wallis, 1952). This test was selected instead of the classical analysis of variance because assumptions of the latter were not met by the datasets.

Table 3
Soil salinity (EC_e) for the 0–0.3, 0.3–0.6, 0.6–0.9, 0.9–1.2, and 1.2–1.5 depth increments at 267 soil sampling locations.

Depth (m)	EC_e (dS m^{-1})				
	0–0.3	0.3–0.6	0.6–0.9	0.9–1.2	1.2–1.5
Mean	7.5	10.5	13.3	14.9	14.1
Minimum	0.4	0.4	0.3	0.4	0.6
Maximum	67.3	38.3	43.8	58.2	42.6
Standard deviation	9.4	8.5	8.6	10.3	9.6

Table 4
Mean, range, and standard deviation for 267 soil sampling locations for soil salinity (EC_e), percent water content on a gravimetric basis (WC), saturation percentage (SP), pH of the saturation extract for the 0–1.2 m soil profile, and apparent soil electrical conductivity for the 0–0.75 (EC_aH), and 0–1.5 m (EC_aV) profile.

	EC_e (dS m^{-1})	WC (%)	SP (%)	pH	EC_aH (dS m^{-1})	EC_aV (dS m^{-1})
Mean	11.6	21.5	70.5	7.9	1.4	2.1
Minimum	0.4	2.5	30.4	6.8	0.1	0.1
Maximum	38.6	49.9	102.7	9.0	5.6	6.8
Standard deviation	8.1	6.3	16.9	0.4	0.9	1.1

2.4. Soil type, crop type, and meteorological settings

According to the US Natural Resources Conservation Service (NRCS) Soil Survey Geographic database (SSURGO), the soil Orders at the selected study fields were: Entisols (43% of the EC_e^* sites), Mollisols (38%), Vertisols (10%), Ardosols (6%), and Inceptisols (3%).

According to the CropScape online database (Han et al., 2012) and data provided by farmers, for each year of the study, the selected fields were farmed with a variety of annual crops, including: alfalfa (*Medicago sativa* L.), cotton (*Gossypium* sp.), garlic (*Allium sativum* L.), maize (*Zea mays* L.), melon (*Cucumis melo* L.), oats (*Avena sativa* L.), onion (*Allium cepa* L.), pistachio (*Pistacia vera* L.), safflower (*Carthamus tinctorius* L.), tomato (*Solanum lycopersicum* L.), triticale (×*Triticosecale* W.), and winter wheat (*Triticum aestivum* L.). Some fields were also kept as pasture and fallow.

Meteorological data were obtained from 34 monitoring stations located across the WSJV and operated by the California Irrigation Management Information System (CIMIS). In particular this study analyzed the effects of precipitation, solar radiation, vapor pressure, air temperature, air relative humidity, wind speed, and soil temperature on the variability of the relationship between soil salinity and the L7 data from 2007 and 2013. The meteorological data were averaged in order to obtain a regional annual value for all variables. Of all meteorological data, rainfall generally shows the most spatial heterogeneity (Tardivo, 2014). Precipitation data from all 34 stations showed correlations beyond the $p < 0.01$ level ($r = 0.76$ or above), suggesting fair homogeneity of meteorological conditions existed throughout the entire WSJV.

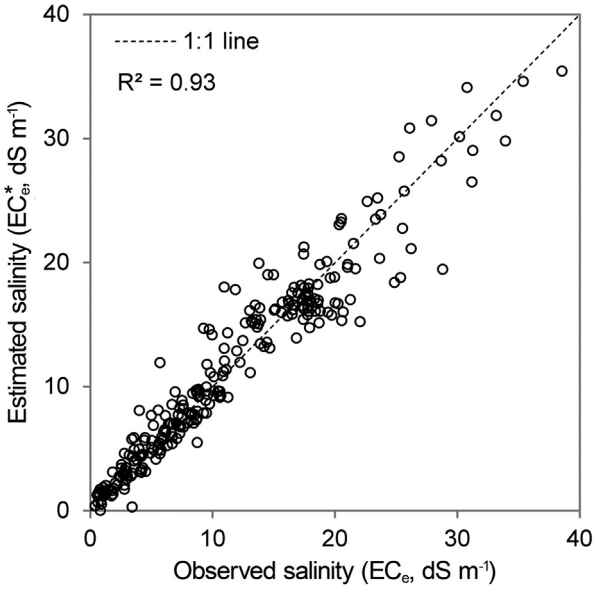

Fig. 2. Scatter plot of soil salinity (EC_e) at 267 sampling locations and estimated salinity (EC_e^*) values using the apparent electrical conductivity (EC_a) readings.

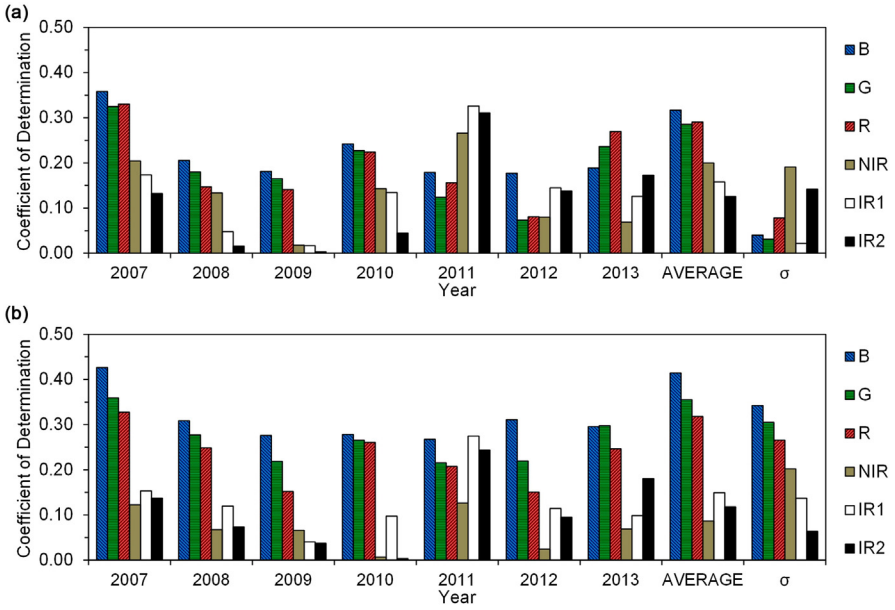

Fig. 3. Coefficients of determination (R^2) between soil salinity from the (a) EC_e and (b) EC_e^* datasets with the blue (B), green (G), red (R), near-infrared (NIR), infrared 1(IR1), and near infrared 2 (IR2) Landsat 7 bands for each single year and for their 7-year average and temporal variability (σ). (For interpretation of the references to color in this figure legend, the reader is referred to the web version of this article.)

3. Results and discussion

3.1. Ground-truth soil salinity

Tables 3 and 4 report the mean and range statistics for soil EC_e at the single and composite depth increments, and the EC_aH and EC_aV readings at the 267 soil sampling locations. For all depth increments, about 50% of the EC_e values were <8 dS m^{-1}, the range in which many crops can grow without substantial yield loss (Maas, 1996). Correlations between depth increments were all positive and significant beyond the $p < 0.01$ level. Correlations between EC_a and EC_e were also significant ($p < 0.01$) at all depths. The best correlations were observed between EC_a and salinity of the 0–1.2 m soil profile, with $r = 0.80$ and 0.85 for EC_aH and EC_aV, respectively. The EC_e values from the 0–1.2 m soil profile showed $r = 0.12$, 0.49, and 0.25 with WC, SP, and pH from the same average depth increment. Soil pH was as high as 9 (Table 4) indicating the likely presence of sodic soils, moreover its low relationship with EC_e suggests that part of the sodic soils could be in the low salinity range (i.e., <4 dS m^{-1}). Non- and slightly saline sodic soils could possibly bias the L7 salinity relationships as common crops hardly grow in such soils.

A second ground-truth dataset, EC_e^*, was estimated with 22 different regressions (one for each field) and characterized by an overall cumulative R^2 of 0.93 (Fig. 2) and root mean square error of 1.92, 3.26, 3.47, 3.76, and 5.41 dS m^{-1} in the 0–2, 2–4, 4–8, 8–16, and >16 dS m^{-1} salinity intervals, respectively. The goodness-of-estimation is fairly high relative to other regional-scale EMI data calibrations (Lobell et al., 2010; Corwin and Lesch, 2014). Corwin and Lesch (2014) indicated that, within the same region, regressions between EC_a and EC_e have very similar slope values, whereas intercepts often change from field-to-field due to edaphic factors that influence EMI reading at small scale. In support of those findings, it is interesting to note that the intercepts of the 22 regression models correlated with average soil properties observed at each field, showing significant ($p < 0.05$) Pearson r values with WC ($r = 0.41$) and SP ($r = 0.51$). Both WC and SP (e.g., indirect measurements of textural properties and bulk density) are known to influence EC_a readings (Corwin and Lesch, 2005). The average slopes were 5.8 and 7.8, with standard deviations of 3.4 and 5.8 for the regressions using EC_aH and EC_aV, respectively. Such standard deviation values suggest that the WSJV might be too large of a region for the application of the methodology developed by Corwin and Lesch (2014).

Once interpolated onto a 30-m block support, EC_e^* was available at 5891 locations. The interpolated EC_e^* values were distributed across the considered salinity intervals such that 15.1, 23.4, 23.8, 30.6, and

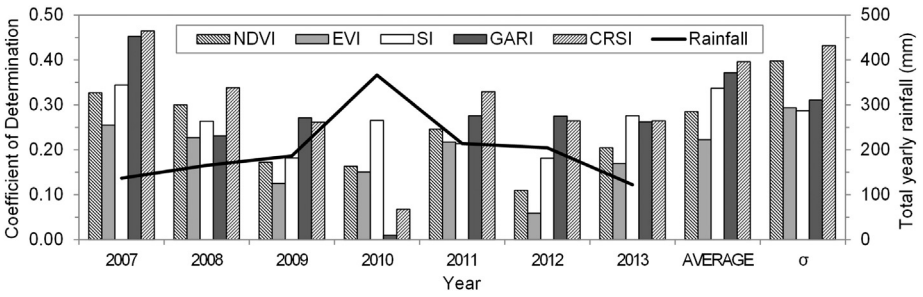

Fig. 4. Coefficients of determination (R^2) between soil salinity from the EC_e^* dataset and selected vegetation indices for each single year and for their 7-year average and temporal variability (σ). The indices considered are the Normalized Difference Vegetation Index (NDVI), the Enhanced Vegetation Index (EVI), the Salinity Index (SI); the Green Atmospherically Resistant Vegetation Index (GARI), and the Canopy Response Salinity Index (CRSI). The black line represents the total yearly rainfall across the western San Joaquin Valley.

7.1% of the values were in the 0–2, 2–4, 4–8, 8–16, and >16 dS m^{-1} ranges, respectively.

3.2. Multi-year Landsat 7 reflectance vs. soil salinity

Fig. 3 shows the coefficients of determination (R^2) between EC_e (Fig. 3a) and EC_e^* (Fig. 3b) versus the various Landsat 7 bands. The B, G, R, IR1 and IR2 reflectance showed positive Pearson correlations with salinity throughout all 7 years. On the other hand, NIR reflectance always showed negative r values. With respect to EC_e (Fig. 3a), the best correlations were generally achieved with the B, G, and R bands. The best correlations for those bands were observed in 2007, with $R^2 = 0.36, 0.32, 0.33$ for B, G, and R, respectively. In 2011, however, the visible bands were outperformed by the NIR and infrared bands, with $R^2 = 0.27, 0.33$, and 0.31 for NIR, IR1, and IR2, respectively. Similarly to EC_e, the best correlations for EC_e^* (Fig. 3b) were observed in 2007 with the B, G, and R bands ($R^2 = 0.43, 0.36$, and 0.33, respectively). The correlations of EC_e^* with the NIR and the infrared bands were generally lower than those with the B, G, and R bands, except in 2011, when IR1 was characterized by the stronger relationships ($R^2 = 0.28$), followed by B ($R^2 = 0.27$), IR2 ($R^2 = 0.24$), G ($R^2 = 0.22$), R ($R^2 = 0.21$), and NIR ($R^2 = 0.13$). Overall, EC_e^* showed stronger relationships with reflectance in all six bands. Regardless of this difference, the R^2 of the L7 bands with EC_e were significantly ($p < 0.01$) correlated (across the 7-year time series) with those for EC_e^*, indicating consistency of results within the two ground-truth datasets. Pearson r values were 0.88, 0.93, 0.92, 0.98, 0.97, and 0.99 for the B, G, R, NIR, IR1 and IR2 bands, respectively.

When compared at the 267 cells overlaying the soil sampling locations (not shown), the relationships between the L7 data and EC_e^* were stronger (on average 68% of the time through the 7 years) than those with EC_e. In particular, the use of EC_e^* over EC_e helped to explain up to an additional 9% of variance for the six L7 bands. This evidence indicates that: *a*) spatial variability existed within the 30 × 30 m pixels, with the interpolated EC_a geospatial measurements better describing soil variability at that spatial scale (i.e., a single soil sample should not be used to represent areas as large as 30 × 30 m); and *b*) the spatial resolution of L7 data might not be enough for properly characterizing the spatial variability of soil salinity in the WSJV. Because of the stronger correlations, this manuscript will focus mainly on the relationships between L7 and EC_e^*. Additionally, hereafter EC_e^* will be referred as soil salinity.

The average and the temporal variability (Fig. 3b) of L7 reflectance over the 7-year period exhibited relatively strong relationships with soil salinity. The 7-year average reflectance generally outperformed the temporal variability with $R^2 = 0.41, 0.36, 0.32, 0.09, 0.15$, and 0.12 for the B, G, R, NIR, IR1 and IR2 bands, respectively. These R^2 values were close to or greater than those observed in the best single year (i.e. 2007). Indeed, as also observed in other regions (Lobell et al., 2010; Scudiero et al., 2014), differences in reflectance between consecutive years were remarkable. Consequently, remote sensing data from a single (random) year should not be used when trying to map salinity, as the risk of producing poor results is clear.

Fig. 4 presents the coefficient of determinations for the selected vegetation indices with EC_e^*, over the 7-year period. Because soil salinity had a negative impact on crop health, the Pearson correlations with EC_e^* were positive for SI (i.e., higher reflectance in the visible range), and negative for NDVI, EVI, GARI, and CRSI (i.e., higher reflectance in the visible range and lower in the NIR). The selected vegetation indices performed with great variations over time. The GARI and the CRSI generally performed better than the other indices. They showed, however, a big drop in performance in 2010. This was likely due to the poor correlation of NIR with salinity in that year (Fig. 3b). For NDVI and EVI, performances in 2010 were not as drastically influenced by NIR. Over the 7-year time, NDVI performed better than EVI, contrary to the results of Lobell et al. (2010). Indeed, the relative performance of vegetation indices depends on many factors, including geographical location, type of satellite sensor, and atmospheric corrections applied to the sensor data when obtaining the actual surface reflectance (Hadjimitsis et al.,

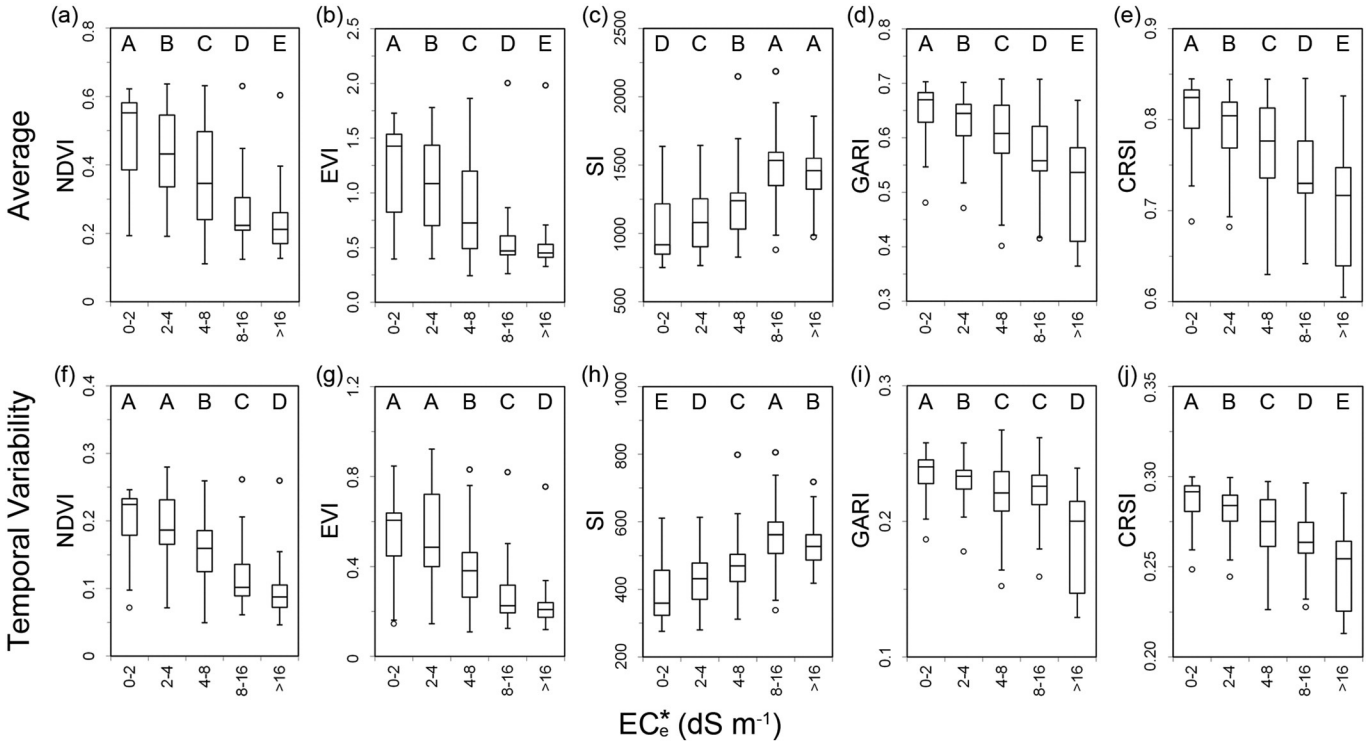

Fig. 5. Boxplots for the 7-year average (top) and temporal variability (bottom) of the Normalized Difference Vegetation Index (NDVI), Enhanced Vegetation Index (EVI), Salinity Index (SI), Green Atmospherically Resistant Vegetation Index (GARI), and Canopy Response Salinity Index (CRSI). The bold line crossing the rectangles represents the median value; circles represent outliers. Within plots, boxes topped with the same letter are not significantly different ($p < 0.05$).

2010; Allbed and Kumar, 2013). Unfortunately, this suggests it may be necessary to identify the best vegetation index for each study, which will increase processing time.

When the 7-year average and temporal variability of the indices were considered, better correlations with salinity were generally observed compared to those for single years. The temporal variability of NDVI and CRSI were characterized by the highest coefficients of determination among the vegetation indices (R^2 of 0.40 and 0.43, respectively). As a rule of thumb, only up to half of the yield spatial variability is influenced by soil properties (Corwin et al., 2003; McBratney et al., 2005; Scudiero et al., 2013). The remaining yield variability comes from factors that normally change from year-to-year (e.g., lack of precipitation, pests, management). The coefficients of determination for the temporal variability of NDVI and CRSI with soil salinity (Fig. 4) should therefore be considered fairly high. For comparison, Scudiero et al. (2014) studied the 3-year temporal variability of corn reflectance in an area characterized by contrasting soils and affected by multiple stress types, including salinity and water stress. They observed that NDVI temporal variability could be used to identify (qualitatively) saline areas, but could only account for a small amount of its variations ($R^2 = 0.11$) due to the biasing effects of other abiotic stresses constantly occurring over time. Those findings highlighted some of the limitations of the approach presented in this study, which can be optimally used in regions where soil salinity is the sole persistent stress occurring over the years, whereas other stress types emerge sporadically and/or with different spatial patterns from time-to-time.

3.2.1. Landsat 7–salinity relationships at selected salinity ranges

The reflectance data could also be used for a qualitative classification of soil salinity at each L7 pixel. The selected salinity ranges (i.e., 0–2, 2–4, 4–8, 8–16, and over 16 dS m^{-1}) were generally characterized by different ($p < 0.01$) values of the 7-year average and temporal variability of the vegetation indices (Fig. 5), and of the six spectral bands (not shown). With the exception of the temporal variability of GARI, high (>8 dS m^{-1}) and low salinity were characterized by significantly different values of the vegetation indices. When focusing on the low salinity ranges, the temporal variability of NDVI and EVI provided the worst performances, as the 0–2 (non-saline) and 2–4 dS m^{-1} (slightly saline) ranges were not characterized by significantly different values of these indices. It is probable that plants were not stressed over this range of salinity; therefore, salinity would have negligible, or positive (see Section 3.2.4), effects on canopy status in the <4 dS m^{-1} range. Additionally, it is also probable that the poor performances at low salinity were due to the saturation of the satellite data, especially in the R band (Gitelson, 2004). Signal saturation is usually observed in the healthier portion of the vegetation once soil is completely covered, making it hard to distinguish slightly stressed plants from non-stressed ones.

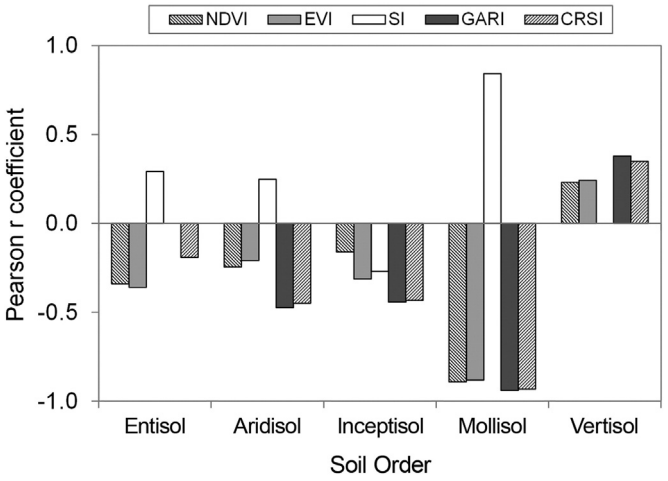

Fig. 6. Pearson r coefficients between soil salinity from the EC_e^* dataset and the 7-year average of the selected vegetation indices according to soil Order. The indices considered are the Normalized Difference Vegetation Index (NDVI), the Enhanced Vegetation Index (EVI), the Salinity Index (SI), the Green Atmospherically Resistant Vegetation Index (GARI), and the Canopy Response Salinity Index (CRSI). All reported correlations are significant at the $p < 0.05$ level.

3.2.2. Changes in the Landsat 7–salinity relationships according to meteorological settings

Meteorological conditions could explain part of the variations in the L7–salinity relationships between 2007 and 2013. The total yearly rainfall (mm) across the WSJV is depicted in Fig. 4. The R^2 values between

Table 5
Correlation matrix for the coefficients of determination of the Landsat 7–EC_e^* relationships (at the cells including the soil sampling locations) and the number of soil sampling location per field, field average ground-truth salinity from the EC_e^* dataset, field average water content (WC), field average soil saturation percentage (SP), and field average pH observed at each field. Bold numbers are significant at the $p < 0.05$ level.

Landsat 7[a]	Number of soil samples	EC_e^*	WC	SP	pH
B	0.19	**0.49**	−0.03	0.28	−0.11
G	0.11	**0.41**	0.19	**0.49**	−0.16
R	0.00	**0.39**	0.01	0.33	−0.07
NIR	−0.12	0.29	0.26	0.10	0.06
IR1	−0.16	0.23	−0.28	−0.16	0.23
IR2	0.09	**0.44**	−0.34	0.05	0.22
NDVI	0.17	0.05	**−0.42**	−0.30	0.03
EVI	0.17	0.19	**−0.38**	−0.16	0.00
SI	0.06	**0.41**	0.10	**0.42**	−0.12
GARI	0.22	−0.06	−0.15	−0.16	−0.16
CRSI	0.21	−0.05	−0.03	−0.08	−0.20
σ(B)	−0.34	−0.24	**−0.47**	−0.33	0.02
σ(G)	−0.18	−0.19	**−0.39**	−0.30	−0.08
σ(R)	−0.05	−0.17	**−0.42**	−0.35	−0.19
σ(NIR)	−0.31	−0.28	**−0.59**	**−0.47**	0.02
σ(IR1)	−0.23	−0.19	**−0.48**	**−0.38**	−0.08
σ(IR2)	−0.24	−0.20	**−0.57**	**−0.46**	0.03
σ(NDVI)	0.01	−0.21	−0.13	−0.14	−0.28
σ(EVI)	−0.05	−0.25	0.02	−0.16	−0.37
σ(SI)	−0.09	−0.18	**−0.43**	−0.36	−0.14
σ(GARI)	−0.13	−0.30	0.14	−0.07	−0.25
σ(CRSI)	−0.11	−0.28	0.07	−0.09	−0.18

[a] Seven-year average of the blue (B), green (G), red (R), near-infrared (NIR), infrared 1(IR1), infrared 2 (IR2), Normalized Difference Vegetation Index, (NDVI), Enhanced Vegetation Index (EVI), Salinity Index (SI), Green Atmospherically Resistant Vegetation Index (GARI), and Canopy Response Salinity Index (CRSI), and their temporal variability (σ).

Table 6
Correlation matrix for the selected vegetation indices[a] and the ground-truth salinity from the EC_e^* dataset, according to crop type/field cover, as reported in the CropScape database (Han et al., 2012) and by the farmers, through the 7-year period. Non-significant (n.s., $p \geq 0.05$) correlations are not reported.

Crop (salt sensitivity[b])	NDVI	EVI	SI	GARI	CRSI
Alfalfa (MS)	−0.32	−0.07	0.39	−0.28	−0.30
Cotton (T)	−0.69	−0.59	0.75	−0.83	−0.82
Garlic (MS)	−0.62	−0.58	0.23	−0.68	−0.67
Maize (MS)	0.49	0.38	−0.66	0.36	0.41
Melon (MS)	n.s.	0.19	0.16	−0.24	−0.19
Oats (T)	0.62	0.63	−0.60	0.59	0.60
Onion (S)	−0.45	−0.37	−0.08	−0.65	−0.63
Pistachio (MS)	0.12	0.17	−0.15	n.s.	n.s.
Safflower (MT)	−0.14	−0.36	0.22	0.53	0.50
Tomato (MS)	n.s.	n.s.	−0.09	n.s.	n.s.
Triticale (T)	0.59	0.56	n.s.	0.58	0.60
Winter wheat (MT)	−0.62	−0.57	0.61	−0.23	−0.48
Fallow	−0.05	0.07	0.32	−0.20	−0.18
Pasture	−0.20	−0.05	0.16	−0.27	−0.30
Non-reported	−0.07	−0.06	0.24	−0.04	−0.04

[a] Normalized Difference Vegetation Index, (NDVI), Enhanced Vegetation Index (EVI), Salinity Index (SI), Green Atmospherically Resistant Vegetation Index (GARI), and Canopy Response Salinity Index (CRSI).
[b] S, sensitive; MS, moderately sensitive; MT, moderately tolerant; T, tolerant.

vegetation indices and EC_e^* were all negatively influenced by rainfall, although the R^2 of GARI and CRSI were the only ones significantly affected ($p < 0.01$), with $r = -0.84$ and -0.80, respectively. It is possible that the high rainfall (e.g., 366 mm in 2010) diluted salinity in the root zone, therefore, mitigating salt stress and negatively impacting the EC_e^*–L7 relationships. Scarce rainfall could also have facilitated the occurrence of water stress, improving the relationships between the vegetation indices and salinity (Letey and Dinar, 1986; Allen et al., 1998). To better understand this effect, information on soil–water availability at each field throughout the 7-year period would be needed, but unfortunately such data are not available and impractical to obtain.

Weaker, yet significant correlations were observed with average minimum air temperature (not collinear with rainfall) through the seven years (8.0, 8.2, 8.4, 8.6, 7.9, 8.6, 8.1 °C in 2007, 2008, 2009, 2010, 2011, 2012, and 2013, respectively). Specifically, the R^2 values of EC_e^* and NDVI, EVI, GAVI, and CRSI were significantly ($p < 0.05$) reduced by temperature, with $r = -0.78$, -0.82, -0.62, -0.72, respectively.

3.2.3. Changes in the Landsat 7–salinity relationships according to soil type

Table 5 shows the correlation matrix for the coefficients of determination of the L7–EC_e^* relationships (at the 267 soil sampling locations) and average values of EC_e^*. The results suggest that the higher the average salinity (EC_e^*) of a field, the stronger some of EC_e^* relationships with the seven-year average reflectance at the B, G, R, and IR2 bands, and with the SI vegetation index, indicating that remote sensing of salinity should always be trained over multiple fields with broad ranges of soil salinity. Otherwise, the results could be biased by the local characteristics of a particular site.

Fig. 6 depicts how the EC_e^* relationships with the average vegetation indices vary according to soil Orders. Canopy reflectance over Mollisols was characterized by very strong relationships ($p < 0.01$) with EC_e^*, with Pearson r values = 0.84 for SI and <−0.88 for the other vegetation indices. Mollisols were characterized by a very wide range of EC_e^* (0.03 to 35.2 dS m^{-1}, average = 8.7 dS m^{-1}, standard deviation = 6.9 dS m^{-1}), as were Aridosols (0.01 to 34.3 dS m^{-1}, average = 7.6 dS m^{-1}, standard deviation = 6.1 dS m^{-1}), although the latter exhibited weaker EC_e^*–L7 relationships. Unexpected relationships were observed over Vertisols, with the correlations for NDVI, EVI, GARI, and CRSI being all positive. Conversely, the salinity–L7 correlations for NDVI, EVI, GARI, and CRSI were all negative and significant ($p < 0.01$) for Inceptisols. Vertisols were characterized by a fairly high average EC_e^* (5.2 dS m^{-1}, range = 0.01 to 11.2 dS m^{-1}, standard deviation = 2.1 dS m^{-1}) relative to that of Inceptisols (1.7 = dS m^{-1}, range = 0.01 to 3.2 dS m^{-1}, standard deviation = 0.6 dS m^{-1}). Multiple factors might be responsible for such diverse relationships (additionally to the properties that identify each Order) including: soil water availability (related to soil textural properties and terrain elevation/slope) and anthropogenic factors (e.g., crop and irrigation management strategies).

In order to help quantify the changes in the L7–EC_e^* relationships due to soil type, Table 5 reports the coefficients of determinations according to field-average WC and SP values. Both WC and SP are related to soil textural or physical properties that affect plant growth through their impact on water and nutrient availability. Table 5 shows that the higher the WC (e.g., higher clay content), the weaker the EC_e^* relationships with the average NDVI and EVI, and with the temporal variability of B, G, R, NIR, IR1, IR2, and SI. Similarly, the higher the field average SP (e.g., higher clay content), the weaker the relationships of salinity with the average G and SI, and with the temporal variability of NIR, IR1, and IR2.

3.2.4. Changes in the Landsat 7–salinity relationships according to crop type

Different crops are expected to be characterized by different L7–salinity relationships, due to different salt tolerance (Maas, 1996) and reflectance properties (Arafat et al., 2013; Mulla, 2013) that characterize different crops. Table 6 reports the correlation matrix between salinity from the EC_e^* dataset and the five selected vegetation indices, through the entire 7-year period. Most of the correlations are significant ($p < 0.05$) and negative. In particular, the GARI and the CRSI performed generally better than the other indices (by 1.6 and 2.0%, respectively). The best performances were observed for GARI and CRSI in fields cropped with cotton, garlic, and onion. Cotton is relatively salt tolerant (Maas, 1996), with yield decreases expected at EC_e levels greater than the threshold value of 7.7 dS m^{-1}. Cotton was, however, grown in soils with EC_e^* ranging between 0.1 and 19.7 dS m^{-1}, and therefore subjected to yield loss due to salinity stress. Contrarily, onion and garlic are, respectively, sensitive and moderately sensitive to salt stress according to Maas (1996), with yield losses starting from EC_e = 1.2 and 3.9 dS m^{-1}, respectively. Both crops were grown over soils with EC_e^* in the 0.7–9.2 dS m^{-1} range.

Few positive correlations between the vegetation indices and salinity were observed. For CRSI, in particular, positive significant correlations were observed with maize (moderately sensitive), oats (tolerant), safflower (moderately tolerant), and tricale (tolerant). All these crops were grown in soil with average $EC_e^* < 3$ dS m^{-1}. In some crops (e.g., cotton) plant growth can be promoted by slightly saline conditions (Corwin et al., 2003); therefore, the positive correlations between ground-truth salinity and the vegetation indices is to be expected.

4. Conclusions

The results indicate that multi-year Landsat 7 Climate Data Record surface reflectance can be a useful indicator for the spatial variability of soil salinity in California's WSJV. The analysis of multi-year average and temporal variability of the L7 bands and of selected vegetation indices improve the correlations between canopy reflectance and soil salinity, which are generally lower when single-year data are considered. The results suggest that data fusion of the L7 multi-year reflectance with information on meteorological conditions, crop type, and soil properties at each L7 pixel might lead to a reliable salinity prediction model for the entire WSJV. Within the tested vegetation indices, the Canopy Response Salinity Index (CRSI) provided the best goodness-of-fit. However, the performance of the tested vegetation indices should be considered specific to the WSJV and the specific atmospheric correction used on the Landsat 7 CDR surface reflectance.

Unfortunately, one limitation of the use of L7 data for salinity assessment lies in its spatial resolution, which appears to be too coarse to fully represent the actual spatial variability of soil salinity. Given the apparent small-scale variability of soil salinity, the latest generation of multispectral very-high resolution satellite sensors (Mulla, 2013), including the WorldView II and III satellites (Digitalglobe Corp., Longmont, CO, USA) with resolution $<2 \times 2$ m, could possibly be used to map soil salinity with higher precision. Data from very high resolution sensors should also be tested for regional-scale salinity assessment in future studies. Future research should focus on field- and regional-scale studies comparing different satellite sensors, spatial resolutions, and atmospheric corrections to improve soil salinity assessment with remote sensing tools. Potentially improved results would, however, come with the cost of greater processing time and operational expenses involved when finer resolution data are managed (Lobell et al., 2010). Additionally, at the moment, very high resolution reflectance products are fairly expensive, whereas the Landsat data is freely provided by the U.S. Geological Survey.

Land resource managers, producers, agriculture consultants, extension specialists, and Natural Resource Conservation Service field staff would be the beneficiaries of regional-scale maps of soil salinity.

Acknowledgments

The funding for this research was from the Office of Naval Research (3200001344). The authors wish to acknowledge the numerous hours of diligent technical work that were performed in the field and in the

laboratory by several technicians whose efforts and conscientiousness were crucial to obtaining the data presented including Wes Clary, Kevin Yemoto, and Michael Bagtang. The authors specifically acknowledge the dedication and technical professionalism of Wes Clary who was crucial in locating field sites in the San Joaquin Valley, conducting EC_a surveys, and analyzing soil samples.

Appendix A. Supplementary data

Supplementary data associated with this article can be found in the online version, at http://dx.doi.org/10.1016/j.geodrs.2014.10.004. These data include Google maps of the most important areas described in this article.

References

Aldakheel, Y., Elprince, A., Al-Hosaini, A., 2005. Mapping of salt-affected soils of irrigated lands in arid regions using remote sensing and GIS. Proceedings of 2nd International Conference on Recent Advances in Space Technologies (RAST 2005). June 09–11, 2005, Istanbul, Turkey, pp. 467–472.

Allbed, A., Kumar, L., 2013. Soil salinity mapping and monitoring in arid and semi-arid regions using remote sensing technology: a review. Adv. Remote Sens. 2, 373–385.

Allen, R.G., Pereira, L.S., Raes, D., Smith, M., 1998. Crop evapotranspiration. Guidelines for computing crop water requirements. FAO Irrigation and Drainage Paper 56. FAO, Rome, Italy.

Arafat, S.M., Aboelghar, M.A., Ahmed, E.F., 2013. Crop discrimination using field hyper spectral remotely sensed data. Adv. Remote Sens. 2, 63–70.

Backlund, V.L., Hoppes, R.R., 1984. Status of soil salinity in California. Calif. Agric. 38, 8–9.

Caccetta, P., Dunne, R., George, R., McFarlane, D., 2010. A methodology to estimate the future extent of dryland salinity in the southwest of Western Australia. J. Environ. Qual. 39, 26–34.

Cone, T., 1997. The vanishing valley. San Jose Mercury News Magazine, June 29:9–15.

Corwin, D.L., Lesch, S.M., 2005. Apparent soil electrical conductivity measurements in agriculture. Comput. Electron. Agric. 46, 11–43.

Corwin, D.L., Lesch, S.M., 2013. Protocols and guidelines for field-scale measurement of soil salinity distribution with EC_a-directed soil sampling. J. Environ. Eng. Geophys. 18, 1–25.

Corwin, D.L., Lesch, S.M., 2014. A simplified regional-scale electromagnetic induction—Salinity calibration model using ANOCOVA modeling techniques. Geoderma 230–231, 288–295.

Corwin, D., Lesch, S., Shouse, P., Soppe, R., Ayars, J., 2003. Identifying soil properties that influence cotton yield using soil sampling directed by apparent soil electrical conductivity. Agron. J. 95, 352–364.

Dang, Y., Pringle, M., Schmidt, M., Dalal, R., Apan, A., 2011. Identifying the spatial variability of soil constraints using multi-year remote sensing. Field Crop Res. 123, 248–258.

Engman, E.T., 1999. Remote sensing in hydrology. In: Corwin, D.L., Loague, K., Ellsworth, T.R. (Eds.), Assessment of Non-Point Source Pollution in the Vadose Zone. American Geophysical Union, Washington, DC, USA, pp. 165–177.

Furby, S., Caccetta, P., Wallace, J., 2010. Salinity monitoring in Western Australia using remotely sensed and other spatial data. J. Environ. Qual. 39, 16–25.

Ghassemi, F., Jakeman, A.J., Nix, H.A., 1995. Salinisation of Land and Water Resources: Human Causes, Extent, Management and Case Studies. CAB international, Wallingford, Oxon, UK.

Gitelson, A.A., 2004. Wide dynamic range vegetation index for remote quantification of biophysical characteristics of vegetation. J. Plant Physiol. 161, 165–173.

Gitelson, A.A., Kaufman, Y.J., Merzlyak, M.N., 1996. Use of a green channel in remote sensing of global vegetation from EOS-MODIS. Remote Sens. Environ. 58, 289–298.

Hadjimitsis, D.G., Papadavid, C., Agapiou, A., Themistocleous, K., Hadjimitsis, M., Retalis, A., Michaelides, S., Chrysoulakis, N., Toulios, L., Clayton, C., 2010. Atmospheric correction for satellite remotely sensed data intended for agricultural applications: impact on vegetation indices. Nat. Hazards Earth Syst. Sci. 10, 89–95.

Han, W., Yang, Z., Di, L., Mueller, R., 2012. CropScape: A Web service based application for exploring and disseminating US conterminous geospatial cropland data products for decision support. Comput. Electron. Agric. 84, 111–123.

Huete, A., Didan, K., Miura, T., Rodriguez, E.P., Gao, X., Ferreira, L.G., 2002. Overview of the radiometric and biophysical performance of the MODIS vegetation indices. Remote Sens. Environ. 83, 195–213.

Ivits, E., Cherlet, M., Tóth, T., Lewińska, K., Tóth, G., 2013. Characterisation of productivity limitation of salt-affected lands in different climatic regions of Europe using remote sensing derived productivity indicators. Land Degrad. Dev. 24, 438–452.

Jackson, T.J., Chen, D., Cosh, M., Li, F., Anderson, M., Walthall, C., Doriaswamy, P., Hunt, E., 2004. Vegetation water content mapping using Landsat data derived normalized difference water index for corn and soybeans. Remote Sens. Environ. 92, 475–482.

Janik, G., 2008. Spatial variability of soil moisture as information on variability of selected physical properties of soil. Int. Agrophys. 22, 35–43.

Jiang, Z., Huete, A.R., Didan, K., Miura, T., 2008. Development of a two-band enhanced vegetation index without a blue band. Remote Sens. Environ. 112, 3833–3845.

Johnston, W., Westcot, D., Delmore, M., 2012. San Joaquin Valley, California: A case study. In: Wallender, W.W., Tanji, K.K. (Eds.), Agricultural Salinity Assessment and Management. ASCE Manuals and Reports on Engineering Practices No. 71. ASCE, Reston, VA, USA, pp. 977–1031.

Kruskal, W.H., Wallis, W.A., 1952. Use of ranks in one-criterion variance analysis. J. Am. Stat. Assoc. 47, 583–621.

Lal, R., Iivari, T., Kimble, J.M., 2004. Soil Degradation in the United States: Extent, Severity, and Trends. CRC Press, Boca Raton, FL, USA.

Lesch, S., 2005. Sensor-directed response surface sampling designs for characterizing spatial variation in soil properties. Comput. Electron. Agric. 46, 153–179.

Lesch, S.M., Corwin, D.L., 2008. Prediction of spatial soil property information from ancillary sensor data using ordinary linear regression: model derivations, residual assumptions and model validation tests. Geoderma 148, 130–140.

Lesch, S.M., Rhoades, J.D., Lund, L.J., Corwin, D.L., 1992. Mapping soil salinity using calibrated electromagnetic measurements. Soil Sci. Soc. Am. J. 56, 540–548.

Lesch, S.M., Rhoades, J.D., Corwin, D.L., 2000. ESAP-95 version 2.01 R. User manual and tutorial guide. Research Rpt. 146.

Letey, J., 2000. Soil salinity poses challenges for sustainable agriculture and wildlife. Calif. Agric. 54, 43–48.

Letey, J., Dinar, A., 1986. Simulated crop-water production functions for several crops when irrigated with saline waters. Hilgardia 54, 1–32.

Li, P., Jiang, L., Feng, Z., 2013. Cross-comparison of vegetation indices derived from Landsat-7 Enhanced Thematic Mapper Plus (ETM) and Landsat-8 Operational Land Imager (OLI) sensors. Remote Sens. 6, 310–329.

Lobell, D.B., 2010. Remote sensing of soil degradation: introduction. J. Environ. Qual. 39, 1–4.

Lobell, D.B., Ortiz-Monasterio, J.I., Gurrola, F.C., Valenzuela, L., 2007. Identification of saline soils with multiyear remote sensing of crop yields. Soil Sci. Soc. Am. J. 71, 777–783.

Lobell, D.B., Lesch, S.M., Corwin, D.L., Ulmer, M.G., Anderson, K.A., Potts, D.J., Doolittle, J.A., Matos, M.R., Baltes, M.J., 2010. Regional-scale assessment of soil salinity in the Red River Valley using multi-year MODIS EVI and NDVI. J. Environ. Qual. 39, 35–41.

Maas, E., 1996. Chapter 13, crop salt tolerance. In: Tanji, K.K. (Ed.), Agricultural Salinity Assessment and Management. American Society of Civil Engineers, New York, NY, USA, p. 262.

Masek, J.G., Vermote, E.F., Saleous, N.E., Wolfe, R., Hall, F.G., Huemmrich, K.F., Gao, F., Kutler, J., Lim, T., 2006. A Landsat surface reflectance dataset for North America, 1990–2000. IEEE Geosci. Remote Sens. Lett. 3, 68–72.

McBratney, A., Whelan, B., Ancev, T., Bouma, J., 2005. Future directions of precision agriculture. Precision Agric. 6, 7–23.

Metternicht, G., Zinck, J., 2003. Remote sensing of soil salinity: potentials and constraints. Remote Sens. Environ. 85, 1–20.

Mulla, D.J., 2013. Twenty five years of remote sensing in precision agriculture: key advances and remaining knowledge gaps. Biosyst. Eng. 11, 358–371.

Odeh, I.O., Onus, A., 2008. Spatial analysis of soil salinity and soil structural stability in a semiarid region of New South Wales, Australia. Environ. Manag. 42, 265–278.

Rouse, J., Haas, R., Schell, J., Deering, D., 1973. Monitoring vegetation systems in the Great Plains with ERTS. Third ERTS Symposium. NASA SP-351, pp. 309–317.

Roy, D.P., Ju, J., Kline, K., Scaramuzza, P.L., Kovalskyy, V., Hansen, M., Loveland, T.R., Vermote, E., Zhang, C., 2010. Web-enabled Landsat Data (WELD): Landsat ETM composited mosaics of the conterminous United States. Remote Sens. Environ. 114, 35–49.

Scudiero, E., Teatini, P., Corwin, D.L., Deiana, R., Berti, A., Morari, F., 2013. Delineation of site-specific management units in a saline region at the Venice Lagoon margin, Italy, using soil reflectance and apparent electrical conductivity. Comput. Electron. Agric. 99, 54–64.

Scudiero, E., Teatini, P., Corwin, D.L., Dal Ferro, N., Simonetti, G., Morari, F., 2014. Spatio-temporal response of maize yield to edaphic and meteorological conditions in a saline farmland using ground-based canopy reflectance. Agron. J. 106, 2163–2174.

Singh, G., Bundela, D., Sethi, M., Lal, K., Kamra, S., 2010. Remote sensing and geographic information system for appraisal of salt-affected soils in India. J. Environ. Qual. 39, 5–15.

Taghizadeh-Mehrjardi, R., Minasny, B., Sarmadian, F., Malone, B., 2014. Digital mapping of soil salinity in Ardakan region, central Iran. Geoderma 213, 15–28.

Tanji, K.K., Wallender, W.W., 2012. Nature and extent of agricultural salinity and sodicity. In: Wallender, W.W., Tanji, K.K. (Eds.), Agricultural Salinity Assessment and Management. ASCE Manuals and Reports on Engineering Practices No. 71. ASCE, Reston, VA, USA, pp. 10–25.

Tardivo, G., 2014. Spatial and time correlation of thermometers and pluviometers in a weather network database. Theor. Appl. Climatol. http://dx.doi.org/10.1007/s00704-014-1148-5.

Triantafilis, J., Laslett, G., McBratney, A., 2000. Calibrating an electromagnetic induction instrument to measure salinity in soil under irrigated cotton. Soil Sci. Soc. Am. J. 64, 1009–1017.

Tweed, S.O., Leblanc, M., Webb, J.A., Lubczynski, M.W., 2007. Remote sensing and GIS for mapping groundwater recharge and discharge areas in salinity prone catchments, southeastern Australia. Hydrogeol. J. 15, 75–96.

Vina, A., Gitelson, A.A., Rundquist, D.C., Keydan, G., Leavitt, B., Schepers, J., 2004. Monitoring maize (*Zea mays* L.) phenology with remote sensing. Agron. J. 96, 1139–1147.